

A Synthetic Study into the Nature and Solution of Nonuniqueness in Surface-Wave Inverse Problems

by M. Hosseini* and S. Pezeshk

Abstract The solution of a Rayleigh-wave inverse problem may potentially deviate from the realistic shear-wave velocity structure due to nonuniqueness. To overcome such deviation, it is necessary to understand the source of nonuniqueness and situations that may give rise to the nonuniqueness. In this study, the existence and formation of the nonunique solutions in an inverse problem are demonstrated by modeling the solution space of a synthetic surface-wave inverse problem and investigating the major causes that might engender nonuniqueness, namely (1) the inversion convergence threshold, (2) ambient noise, (3) corner frequency of the recordings, and (4) the water level. Regarding the severity of nonuniqueness in the phase-velocity inverse problems, a technique is proposed to improve the inversion that exploits the match between the synthetic and observed time series used as *a posteriori* information for constraining the realistic velocity structure. Through a synthetic example, the effectiveness of such method is tested and demonstrated effective.

Introduction

Shear-wave velocity (V_S) is an important parameter in site-response analyses for estimating the spectral amplification factor in the field of earthquake engineering (Borcherdt, 1994; Cramer *et al.*, 2002; Pezeshk and Zarrabi, 2005). The thickness and shear-wave velocity of the soil layer and the impedance ratio between bedrock and the soil layer are major input parameters needed to perform site-response analysis.

In reservoir engineering, seismic techniques are frequently used for the characterization of reservoir structure (Hosseini and Aminzadeh, 2013, 2014). Specifically, in hydrocarbon explorations, surface waves can help constrain near-surface velocity structure in a full-waveform seismic inversion and reduce uncertainties in reservoir characteristics in situations in which near-surface logs may not be reliable or available due to washouts during drilling (Bourgoyne *et al.*, 1986; Pan *et al.*, 1994). In addition, near-surface shear-wave velocity structure helps to remove ground roll noise from seismic reflection sections and improves deep seismic imaging reliability (Strobbia *et al.*, 2010, 2011, 2012; Salama *et al.*, 2013). Recently, innovative application of surface-wave analysis for assessment of the geotechnical structures was reported where mechanical properties of a buried geosynthetic material were evaluated (Kafash *et al.*, 2013).

The shallow shear-wave velocity profile at a specific site can be obtained using invasive or noninvasive techniques. Noninvasive techniques include active and passive surface

seismic methods such as multichannel analysis of surface waves (MASW, Park *et al.*, 1999), spectral analysis of surface waves (SASW, Nazarian, 1984; Nazarian and Stokoe, 1986), or refraction microtremor (Louie, 2001) in which vertical variation of mechanical properties of the medium is estimated from spectral variation of phase velocities through the inversion of dispersion curves (Stovall, 2010; Hosseini and Pezeshk, 2011a; Hosseini, 2014).

The shear-wave velocity structure can be estimated by studying the dispersive properties of the surface waves in a vertically heterogeneous medium (Dorman and Ewing, 1962; Brune and Dorman, 1963; Wiggins, 1972). Several approaches are available for the inversion of surface waves, including forward-modeling approaches and the linearized inversion of dispersion curves. Forward-modeling approaches such as genetic algorithms offer an alternative to the traditional linearized inversions and can sample a broader part of the model space (Sambridge, 1999; Mosegaard and Sambridge, 2002; Pezeshk and Zarrabi, 2005; Sambridge *et al.*, 2006); however, the time-consuming nature of these techniques limits their application.

Inversion techniques suffer from limited search scope in the model space. A successful inversion procedure must be able to find solutions near the global optimum; however, such a goal might not be easily attained considering the likely existence of multiple local minima (Cerato, 2009), which will result in nonuniqueness. Several approaches have been proposed to overcome the nonuniqueness, such as using *a priori* information, adjusting inversion parameters, using *a posteriori*

*Now at AECOM Technical Services, Inc., 915 Wilshire Boulevard, Suite 700, Los Angeles, California 90017.

information, and employing joint inversion techniques. Cerato (2009) utilized *a priori* information about the subsurface material to constrain the range of values in the inversion process. Use of higher modes of propagation (Levshin and Panza, 2006; Hosseini and Pezeshk, 2011b, 2012a) and alternative model parameterization (Renalier *et al.*, 2010) are considered as methods that adjust inversion parameters aiding to reduce the nonuniqueness. Methods that exploit *a posteriori* information opt out of the inverted models after the inversion process, such as techniques using the effective phase-velocity dispersion match (Cerato, 2009) and the synthetic and observed seismogram match (Hosseini and Pezeshk, 2012b, Hosseini, 2014; Hosseini *et al.*, 2014). In a joint inversion technique, more data in addition to the dispersion curve are simultaneously inverted to determine the velocity structure, such as in the procedure outlined by Tran and Hiltunen (2012). Joint inversion of the surface waves and the reflection, refraction, and *P*- or *S*-wave travel times are other examples of the joint inversion methods that are frequently reported (Dal Moro and Pipan, 2007).

In this study, the feasibility of using *a posteriori* wave-number integration technique for improving nonuniqueness in the inversion of phase-velocity dispersion curves is evaluated. Unlike a joint inversion that may suffer from having different weights for different data types, the *a posteriori* technique only evaluates the outcome of the inversion for further refinement. To illustrate the need for such a study, the first part of the current study focuses on the mathematical nature of nonuniqueness. The second part of the study is devoted to showing that the selection of parameters in data processing and inversion can give rise to potential nonunique solutions. By studying the model space for a specific velocity profile, it is visually illustrated that some of these nonunique solutions that are not avoidable are random in nature (such as those formed due to the lowest recorded frequency of the time series and ambient noise) and some are avoidable (such as convergence criteria used in inversion). In the following sections, it is shown that the synthetic seismograms are more affected by changes in the velocity structure compared to the phase-velocity dispersion curves. This conclusion forms the strategy proposed to overcome the nonuniqueness using an *a posteriori* technique.

For the rest of the study, we discuss the existence of nonuniqueness in a linearized surface-wave inversion through a synthetic example, and its occurrence is discussed in accordance with the details of the fitness function for the model space. Finally, we use synthetic seismograms to quantitatively select the most appropriate shear-wave velocity profile.

Nonuniqueness in the Inversion

Surface-wave inversion is a nonlinear problem, and available solutions are usually acquired through a linearized inversion technique (Aster *et al.*, 2013). Scientists and engineers relate the physical parameters of a system to the observations.

In engineering and seismology, observations and system parameters are discrete quantities viable to operate as vectors. A forward problem is simply finding the observation having the model parameters, and an inverse problem is the estimation of unknown model parameters given the observations. Inverse problems can be solved using least squares, maximum likelihood, generalized inversion methods, or evolutionary techniques.

The physics of such a system can be represented using a function $\mathbf{G}(\mathbf{m})$ that relates the system parameters to the observations by the general equation:

$$\mathbf{G}(\mathbf{m}) = \mathbf{d}, \quad (1)$$

in which $\mathbf{G}(\mathbf{m})$, which is called the forward operator, maps the model on the observation \mathbf{d} , and \mathbf{m} is the true model. The operator can take different forms, such as a linear or nonlinear system of algebraic, ordinary differential, or partial differential equations (Aster *et al.*, 2013). In the case of a nonlinear forward operator, the perturbation theory (Prosser, 1968; Snieder, 1990a,b) can be used to express data as a perturbation series of the model parameters. In the perturbation theory, the nonlinear problem is linearized for a small region around the true model using the Taylor expansion and neglecting the higher-order terms. In such case, the linearized problem can be presented as

$$\mathbf{G}\mathbf{m} + \mathbf{e} = \mathbf{d}, \quad (2)$$

in which \mathbf{e} is the error contaminating the data (Snieder and Trampert, 2000). Because the number of observations is usually more than the model parameters, the solution to this linear problem is expressed as

$$\tilde{\mathbf{m}} = \mathbf{G}^{-g}\mathbf{d}, \quad (3)$$

in which \mathbf{G}^{-g} is the generalized inverse of \mathbf{G} , and $\tilde{\mathbf{m}}$ is the estimated model different from true model (Snieder and Trampert, 1999).

We employ a singular value decomposition (SVD) technique, which aids in mathematically showing that it is possible to construct nonunique solutions for an inverse problem. It should be noted that the definition of nonuniqueness is beyond what is shown in this section because we provide a special case in which low eigenvalues can contribute to the formation of nonunique solutions.

For each specific solution set $\tilde{\mathbf{m}}$ with n elements, operator \mathbf{G} associated with m observations with size $m \times n$ can be factored into

$$\mathbf{G} = \mathbf{U}\mathbf{S}\mathbf{V}^T, \quad (4)$$

in which \mathbf{S} is a diagonal matrix containing singular values of the operator \mathbf{G} (s_i on its diagonal), has the same size as \mathbf{G} , and is customarily arranged in the descending order. Matrices \mathbf{U} and \mathbf{V} are $m \times m$ and $n \times n$ unitary square matrices, and the columns of each form a set of orthonormal vectors spanning observation data and model space. The superscript T for \mathbf{V} denotes the conjugate transpose. It is possible to

break every model and observation data down into a linear combination of their associated orthonormal vectors:

$$\tilde{\mathbf{m}} = \sum_{i=1}^n g_i \mathbf{V}_{\cdot,i}, \quad \mathbf{d} = \sum_{i=1}^m h_i \mathbf{U}_{\cdot,i}, \quad (5)$$

in which g and h are scalars, and $\mathbf{U}_{\cdot,i}$ and $\mathbf{V}_{\cdot,i}$ are the i th columns of \mathbf{U} and \mathbf{V} . In the \mathbf{S} matrix, some of the singular values might be zero (or relatively very small) and cause an ill-conditioned inverse problem (Aster *et al.*, 2013); such eigenvalues can be separated from the equation by identifying the p th eigenvalue, beyond which eigenvalues are practically assumed to be zero:

$$\begin{aligned} \mathbf{G} &= [\mathbf{U}_{\cdot,1} \mathbf{U}_{\cdot,2} \dots \mathbf{U}_{\cdot,m}] \begin{bmatrix} \mathbf{S}_p & 0 \\ 0 & 0 \end{bmatrix} [\mathbf{V}_{\cdot,1} \mathbf{V}_{\cdot,2} \dots \mathbf{V}_{\cdot,n}]^T \\ &= [\mathbf{U}_p \ \mathbf{U}_0] \begin{bmatrix} \mathbf{S}_p & 0 \\ 0 & 0 \end{bmatrix} [\mathbf{V}_p \ \mathbf{V}_0]^T, \end{aligned} \quad (6)$$

in which \mathbf{U}_p and \mathbf{V}_p are the first p columns in their associated matrices. \mathbf{U}_0 denotes the last $(m-p)$ columns in \mathbf{U} , and \mathbf{V}_0 denotes the last $(n-p)$ columns in \mathbf{V} .

One of the definitions of the nonuniqueness is a non-trivial solution $\tilde{\mathbf{m}}_0$ that projects into null space meaning that $\mathbf{G}(\mathbf{G}\tilde{\mathbf{m}}_0) = 0$. The null space of \mathbf{G} is denoted with $N(\mathbf{G})$, and columns of \mathbf{V}_0 form an orthogonal basis for $N(\mathbf{G})$, meaning that adding any linear combination of \mathbf{V}_0 columns to the solution $\tilde{\mathbf{m}}$ does not project into the data space:

$$\begin{aligned} \tilde{\mathbf{m}} &= \tilde{\mathbf{m}}_{\dagger} + \tilde{\mathbf{m}}_0 = \tilde{\mathbf{m}}_{\dagger} + \sum_{i=p+1}^n g_i \mathbf{V}_{0,i}, \\ \tilde{\mathbf{m}}_{\dagger} &= \mathbf{V}_p \mathbf{S}_p^{-1} \mathbf{U}_p^T \mathbf{d}, \end{aligned} \quad (7)$$

in which $\tilde{\mathbf{m}}$ is a nonunique solution, and $\tilde{\mathbf{m}}_{\dagger}$ is the SVD solution. By varying sets of g_i factors, one can construct sets of nonunique solutions that, for all, equality $\mathbf{G}(\tilde{\mathbf{m}}_{\dagger} + \tilde{\mathbf{m}}_0) = \mathbf{G}(\tilde{\mathbf{m}}_{\dagger}) = \mathbf{d}$ holds.

In addition to small eigenvalues, nonuniqueness can rise due to the nonconvexity of a nonlinear objective function; for instance, the existence of multiple local minima can make the inversion process yield different results based on the starting point in the model space.

Backus and Gilbert (1970) stated that numerical investigation is the only way to study the existence of nonunique solutions for an objective function. In the following section, we numerically simulate the existence of the nonunique solutions for a fairly simple velocity structure. We then examine the existence of nonunique solutions by studying the solution space of the objective function without performing any inversion.

Synthetic Test to Study the Solution Space

It is assumed that there are several items that can give rise to the existence of multiple solutions for a surface-wave inverse problem. These items are intuitively selected from

effects that might deviate from the results of an inversion from the realistic velocity model. They are (1) level of inversion convergence, (2) ambient noise in the recorded data, (3) corner frequency of the recorded data, and (4) the methodology used for handling parameters other than the shear-wave velocity and thickness (such as Poisson's ratio or quality factor). The provided list does not cover all causes of nonuniqueness in the surface-wave inversion; however, it provides an understanding of the complexity of the problem and the nonuniqueness associated with the inverse problems. The cause of the formation of the nonunique solutions is the nonlinearity of the surface-wave forward operator, as observed by the study of the solution space.

To illustrate the role of the aforementioned assumptions on the inversion result, we perform and discuss a comprehensive synthetic test through an example problem. For the synthetic test, we consider a six-layer medium over the half-space. We calculate the theoretical dispersion curves for a range of quantities assigned to each layer. We keep the shear-wave velocities of all layers constant except for the fifth layer and the half-space, for which we use a range of shear-wave velocities between 50 and 700 m/s and between 270 and 850 m/s with 10 m/s increments, forming the model space. We perform simulations assuming (1) there is no attenuation-induced dispersion (Kanamori and Anderson, 1977), i.e., the quality factor for shear and compressional waves is infinite, and (2) the shear-wave velocity of layers does not exceed its value in the half-space. The error space is formed by calculating the difference between the phase-velocity dispersion from the model space and the dispersion for a selected reference model. The reference model is assumed to represent the realistic velocity structure and will be kept constant throughout the study. The shear-wave velocity of the fifth and seventh layers in the reference model is set equal to 270 and 570 m/s, respectively, and a water level on top of layer 3.

We only allow changes to the shear-wave velocity of two layers to be able to visually inspect the effect of such changes on the error space. As presented in Table 1, we consider eight groups of simulations considering various water-table levels at each layer.

Poisson's ratio and density can be used to simulate the effect of water-level existence (Foti and Strobbia, 2002) and consequent material saturation. For dry material, we used a Poisson's ratio of 0.25 and a density of 1.8 g/cm³, and for the saturated material we used 0.45 and 2.1 g/cm³. Water level is shown in Table 1. Considering the ranges introduced for the fifth layer and seventh layer, 2948 different velocity models are used in each simulation set, and a total of 23,584 velocity models are used throughout this study. The properties of all layers except the fifth and seventh layers are fixed.

For each model in Table 1, we determined the associated phase-velocity dispersion curve for the frequency range of 5–100 Hz. We used Computer Programs in Seismology, developed by Robert Herrmann (see Data and Resources), to perform forward calculations. We calculated the residual (the difference between the dispersion curves from each

Table 1
Model Space Considered in This Study

Layer	Thickness (m)	V_S Value/Range (m/s)	Poisson's Ratio and Density Type Simulation Set*								
			1	2	3	4	5	6	7	8	
1	2	100	a	b [†]	b	b	b	b	b	b	b
2	2	100	a	a	b [†]	b	b	b	b	b	b
3	2	175	a	a	a	b [†]	b	b	b	b	b
4	2	240	a	a	a	a	b [†]	b	b	b	b
5	2	50–700 every 10	a	a	a	a	a	b [†]	b	b	b
6	2	265	a	a	a	a	a	a	b [†]	b	b
7	∞	270–700 every 10	a	a	a	a	a	a	a	a	b [†]

*Type (a), saturated material with Poisson's ratio of 0.45 and density of 2.1 g/cm³; type (b), dry material with Poisson's ratio of 0.25 and density of 1.8 g/cm³.

[†]Water level.

velocity model in Table 1 and the reference velocity model) using the following fitness function:

$$\text{Error} = \sum_{j=1}^{\text{NF}} \left[\frac{|c_j^{\text{obs.}} - c_j^{\text{theo.}}|}{c_j^{\text{obs.}}} \times \frac{100}{\text{NF}} \right], \quad (8)$$

in which NF is the number of frequencies, $c_j^{\text{obs.}}$ is the experimental dispersion curve at frequency j , and $c_j^{\text{theo.}}$ is the theoretical dispersion curve. Equation (8) is used only for the fundamental-mode dispersion curve. In calculating the errors, we selected a velocity model as the reference model and treated its associated dispersion curve as the experimental dispersion curve ($c^{\text{obs.}}$). Then, we calculate the error space using equation (8) and study the error space to gain insight into the behavior of an inverse problem.

In the following sections, we investigate the inversion process using the models provided in Table 1 and the reference model. We specifically will study the effects of (1) the level of inversion convergence, (2) noise in the data, (3) the lowest recorded frequency of the recordings, and (4) the methodology for handling parameters other than shear-wave velocity and thickness (i.e., Poisson's ratio).

Effect of Convergence Level

The level of convergence in the inversion is set by two criteria: the maximum number of the iterations or by a threshold error. A large value for the threshold error can cause immature termination. This problem is more evident in cases in which the error space has a gradual gradient with respect to one of the inversion parameters, such as the shear-wave velocity of one of the layers. The effect of the convergence level is explained with numerical simulation via investigation of error space constructed from the model space in Table 1.

The error space is constructed with respect to the phase-velocity dispersion curve of the reference model and is shown as a contour map in Figure 1a, corresponding to the simulation 3 from Table 1. The reference model is shown in Figure 1b along with its associated phase-velocity dispersion curve. The reference model is shown with a circle. As can be observed

from Figure 1a, the shear velocities associated with the minimum error also match those of the reference model, and the inversion is capable of obtaining the true velocity model.

Also observable in Figure 1a, when the water level is assumed to be on top of layer 3, the local minimum and the global minimum are the same; therefore, the choice of initial model does not alter the final outcome of the inversion. According to Figure 1a, regardless of the selection of the initial model, the inversion will converge to the reference model after a sufficient number of iterations. However, the inversion usually is not carried out for a goal of zero threshold error, but instead an error level is selected as an acceptable threshold. This error threshold should ideally be chosen in a manner that model parameters (here $V_{S,5}$ and $V_{S,7}$) result in similar values with the case of a zero threshold error, although this might not be possible. In Figure 1a, models falling on the boundaries of the region marked with the bold-dashed line have errors equal to 0.15%. Two models are selected that have a threshold error of 0.15%, marked with two open triangles in Figure 1. The model corresponding to triangle 1 is very different than the reference model illustrated with a filled circle; however, the model corresponding to triangle 2 is close to the reference (Fig. 1b).

This implies that when a threshold is selected, it becomes important what path is taken toward the optimal solution in the inversion process. For instance, if an initial model is in region A of Figure 1a, the slow gradient will result in an inverted model that is different than the case in which an initial model is selected in region B with a sharp gradient toward the reference model.

Effect of Noise

The same analysis is repeated by adding 10% random uniform noise to the phase-velocity dispersion data from the reference model (Fig. 2). The error space in Figure 2 is recalculated assuming a known water level. The coordinates of the minimum-error model and the reference model are presented with an X and a circle in Figure 2a. It can be observed that the existence of 10% noise dramatically influ-

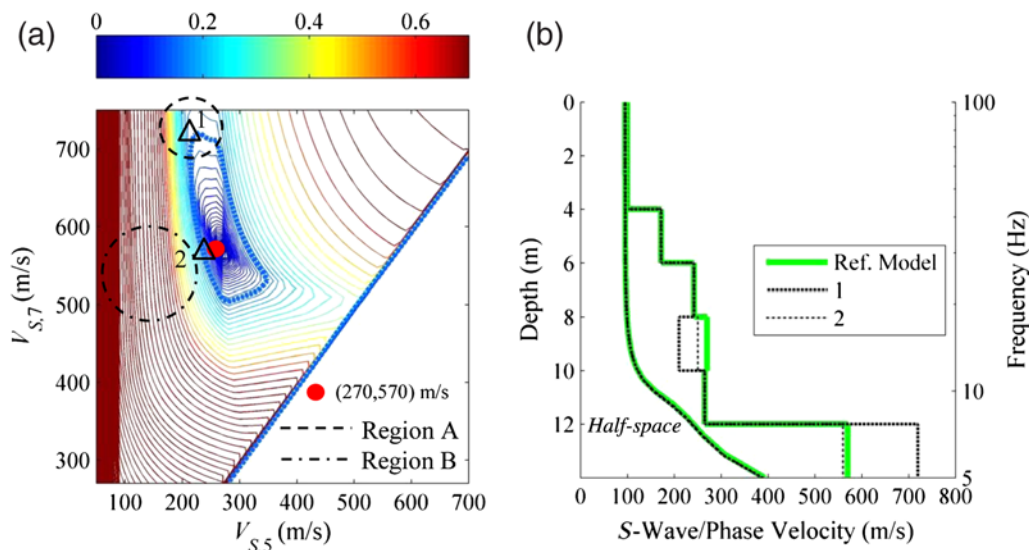


Figure 1. (a) The contour map of equation (8), corresponding to the simulation 3 of Table 1. (b) Shear-wave velocity model and phase-velocity dispersion curves corresponding to points 1 and 2 in (a), respectively. The circle in the contour plot is the coordinate of V_S for the fifth and seventh layers of the reference model and is associated with the minimum error. Triangles numbered 1 and 2 are two models with similar errors and are expected to be the result of inversion if the initial model is located in the area enclosed by the circles in the vicinity of each model. The color version of this figure is available only in the electronic edition.

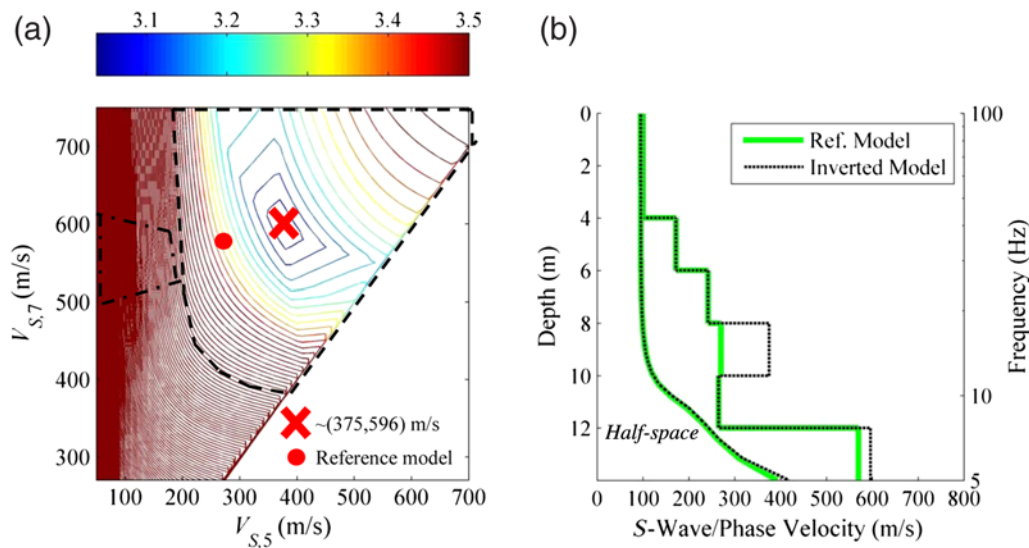


Figure 2. (a) Objective function contours (equation 8) are calculated for the solution space from simulation 3 (Table 1) with respect to dispersion from the reference model with 10% noise. (b) Shear-wave velocity model and phase-velocity dispersion curve for the reference and inverted model. The circle in the contour plot is the coordinate of the fifth and seventh layers' V_S for the reference model, and coordinates of the X symbol represent the $V_{S,5}$ and $V_{S,7}$ of the minimum of the objective function. The polygon with dashed-bold line in Figure 2a corresponds to a 4% error. The color version of this figure is available only in the electronic edition.

ences the inverted shear-wave velocity at the fifth layer to increase about 40% (inverted value of about 375 m/s versus the accurate value from the reference model equal to 270 m/s).

It is necessary to recall that the ultimate inversion solution shown in Figure 2a with an X corresponds to a minimum error in the error space of Figure 2. This point will be reached only if the inversion is allowed to reach its minimum possible error, which is not practical. Similar to the previous section, threshold error is selected in a way that is slightly

higher than minimum error. A value of 4% is selected as the threshold error. Models on the boundaries of the polygon with the dashed-bold line in Figure 2 correspond to the possible results of inversion with 4% threshold error. These models show a broad variation in shear-wave velocities and such an error threshold makes the inversion somehow impractical for identifying the reference model from the current error space. In Figure 2a, coordinates of the reference model show that it is possible to get close to the reference

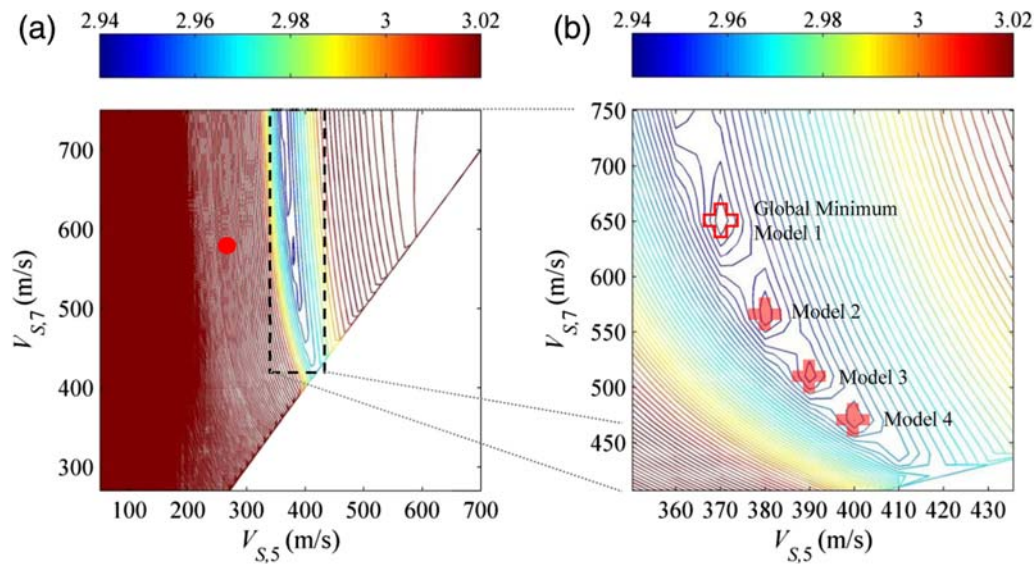


Figure 3. (a) Objective function contours (equation 8) are calculated for the solution space from simulation 3 (Table 1) with respect to dispersion from the reference model with 10% noise in which the three lowest frequencies are not used in objective function calculations. (b) The section within the dashed polygon in (a) is enlarged. The circle in the contour plot (a) is the coordinate of the fifth and seventh layers' V_S for the reference model. The color version of this figure is available only in the electronic edition.

model using an initial model in the region bounded by the dashed-dotted polygon; however, existence of *a priori* information is necessary. This region is similar to the suggestion made for the initial models shown in Figure 1.

Effect of Lowest Recorded Frequency

The lower limit of the frequency used in the dispersion is important because it is associated with the resolution of the inverted velocity profile in depth and is a direct function of the recording instrument response, ambient noise, and the low-frequency energy of the active source (Stovall, 2010; Hosseini, 2014). In surface waves, the phase velocities at high frequencies are associated with shallow layers. As frequency decreases, the number (and overall depth) of layers nonlinearly participating to form a specific phase velocity increases.

The error space from the previous section (affected by 10% uniform random noise) is used here. Error space is recalculated by considering frequencies ≥ 8 Hz for calculation of the phase-velocity dispersion curve and their difference with noise-added dispersion data from the reference model (Fig. 3). To attain this, we eliminated three frequencies (5, 6, and 7 Hz) from the dispersion curves for all the models and the reference model. The rectangular block shown in Figure 3a is enlarged and displayed in Figure 3b. As shown in Figure 3b, there are several local minima that make the inversion nonunique and complicated. The local minima are marked by different cross symbols in Figure 3b. The prominent feature of the error space in Figure 3 is the existence of multiple local minima where, depending on the initial model, an inversion can get trapped (Pezeshk and Zarrabi, 2005). Each of the models associated with the local minima can be a solution to the inversion. Using an evolutionary technique such as a genetic

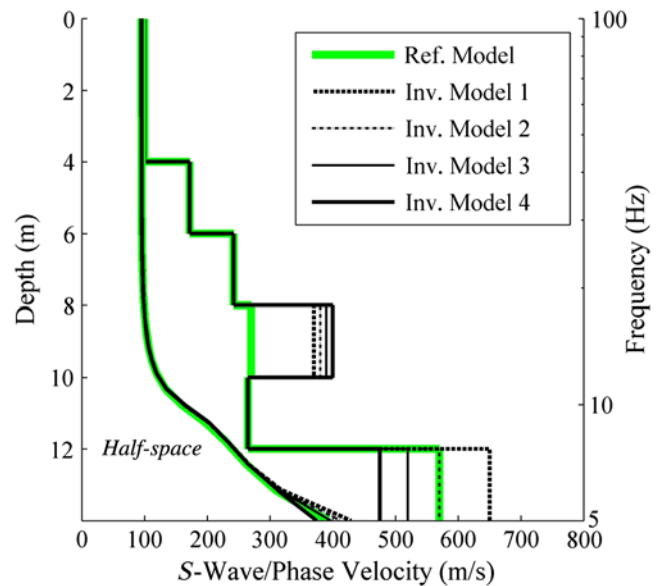


Figure 4. Shear-wave velocity model and phase-velocity dispersion curve are shown for the reference and expected inverted models as shown in Figure 3. The color version of this figure is available only in the electronic edition.

algorithm similar to Pezeshk and Zarrabi (2005), one may identify the global minimum in Figure 3b. However, exclusion of low frequencies has created a global minimum (model with $V_{S,5} = 430$ m/s and $V_{S,7} = 750$ m/s, shown by an open cross in Fig. 3b) which is different than the reference model. Solution models associated with Figure 3 are plotted against the reference model in Figure 4. From Figure 4, it is observed that the lack of low-frequency data has impaired the resolution of inversion in depth. The effect of low-frequency data is sub-

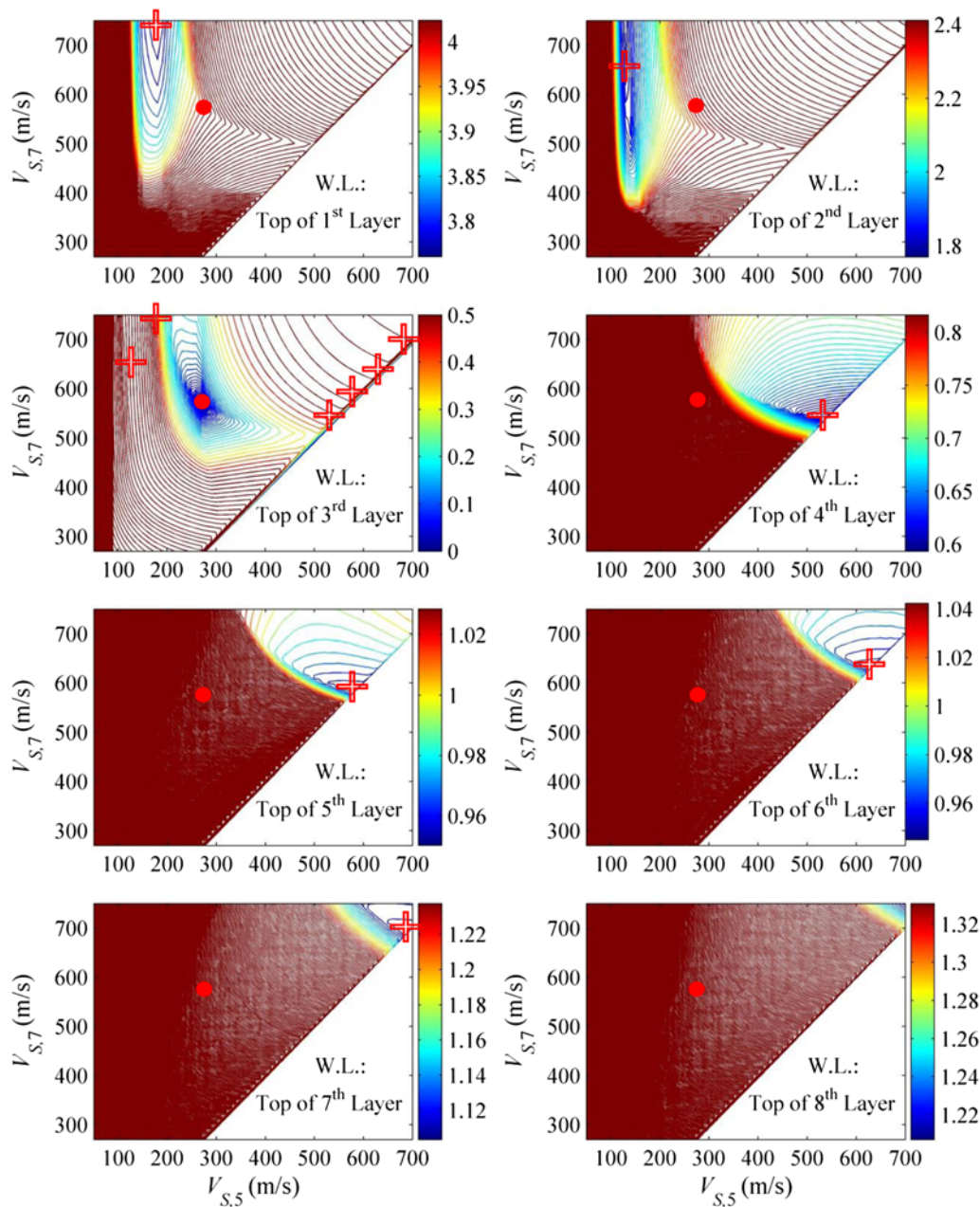


Figure 5. Objective function contours (equation 8) are calculated for the solution spaces from simulations 1–8 with respect to dispersion from the reference model. Circles in the contour plots are the coordinate of the fifth and seventh layer V_S for the reference model with water level (W.L.) on top of layer 3 (simulation 3). Crosses in contours show the minimum of objective function for which the coordinates denote the $V_{S,5}$ and $V_{S,7}$. The color version of this figure is available only in the electronic edition.

stantial, even though the dispersion data from only three frequencies (5, 6, and 7 Hz) are not used among the 52 frequencies. This observation might shed light on the significant contribution from the correct geophone type, sufficiently strong source, and passive techniques for low-frequency treatment.

Water Level Effect: Individually and Combined

Among the layer parameters, shear-wave velocity and thickness are recognized to have the maximum effect on the phase-velocity dispersion data; other parameters such as Pois-

son's ratio (or, subsequently, compressional-wave velocity) have a minor effect (Nazarian and Desai, 1993). In this section, it is shown that various assumptions regarding the water level can dramatically disturb the inversion result, and their effects must be considered in a surface-wave inversion. We perform the calculation for the error space, considering eight different water levels from Table 1. Each of the eight sets of simulations will be performed for noise-free data.

Figure 5 shows the error space for the velocity model introduced in Table 1 and the reference model, where the water level follows that from the simulation sets one to eight.

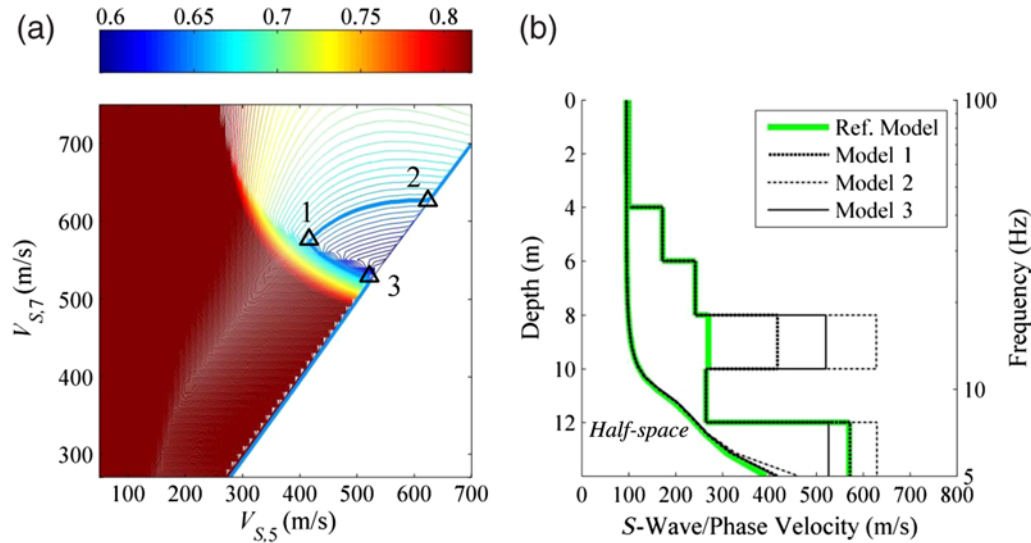


Figure 6. (a) Objective function contours (equation 8) are calculated for the solution space from simulation 4 (Table 1) with respect to the dispersion from the reference model without adding any noise. (b) Shear-wave velocity models and phase-velocity dispersion curves are shown for the reference model and three selected models on the contour. The color version of this figure is available only in the electronic edition.

Each error space in Figure 5 has at least a minimum error, which is marked with a cross. The reference model with which the error space is generated is also indicated in all error spaces with a solid circle to present a visual inspection for the proximity of the minimum-error solution and reference model. In Figure 5, in the error space with the water level on top of layer 3, which is the same water level as the reference model, the minimum-error solution is the same as the reference model. It is observed that the lack of knowledge regarding the water level can affect the accuracy of inversion drastically.

Nonuniqueness Issues

Through several simple example problems, we investigated various parameters that can influence the inversion process and, as a result, the final selection of the shallow shear-wave velocity profile. Other important issues that must be resolved are the nonunique characteristics of the inversion. To be able to use the MASW or SASW procedures confidently and make them practical for engineering applications, we need to resolve the nonuniqueness issue. We resolve this issue by looking at the waveform error space in addition to the phase-velocity dispersion error space.

To achieve such a goal, we choose velocity models that have almost identical error in the phase-velocity error space. Such velocity models can be easily found using a specific isoline in the error space of phase-velocity dispersion. A group of velocity models are chosen from an isoline in the dispersion error space of Figure 6a, with the water level on top of the fourth layer (isoline is marked with a bold line). We select three velocity models on that isoline as displayed in Figure 6b. Then, we generate synthetic seismograms for

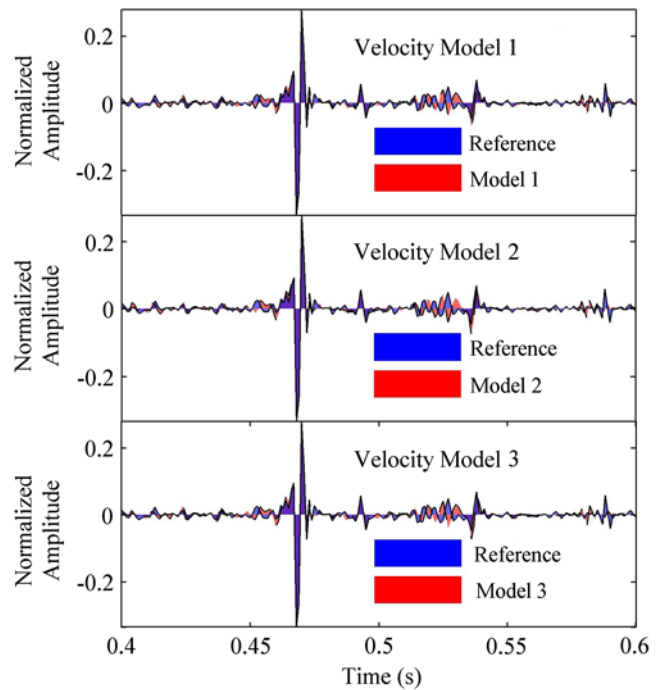


Figure 7. Synthetic time series generated for three velocity models picked from Figure 6, each individually plotted against the synthetic time series from the reference model. The color version of this figure is available only in the electronic edition.

these models and compare these seismograms with the reference model seismograms.

We used the wavenumber integration technique of Wang and Herrmann (1980) to generate full wavefield synthetic seismograms, in which details of the wavefield, such as all direct and scattered body waves and surface waves for a horizontally layered earth model, are present. Figure 7 shows the

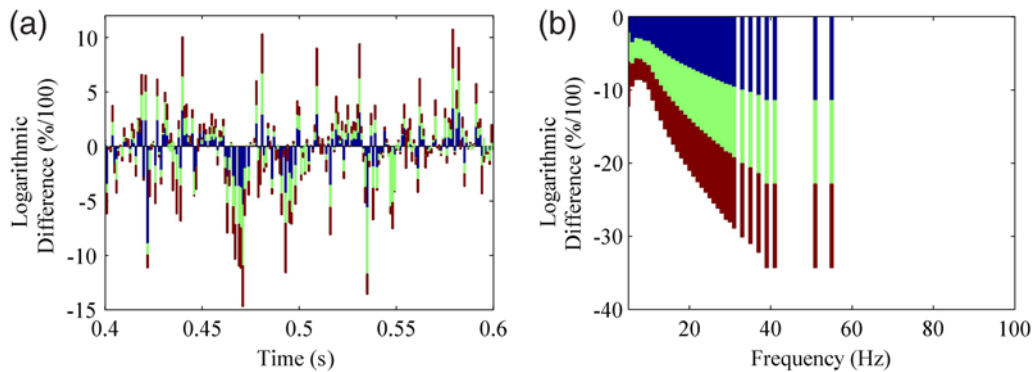


Figure 8. (a) Logarithmic difference between time series from three models (shown in Fig. 6) and that from the reference model. (b) Logarithmic difference between dispersion curves from the three models and that from the reference model. The color version of this figure is available only in the electronic edition.

synthetic times series for each velocity model of Figure 6 along with that of the reference model. For clarity, the Rayleigh wavetrain in Figure 7 is scaled down in time window $\sim[470\ 490]$ ms so that the details of the time series would be clearly visible. Synthetic time series are generated at a constant distance.

To elucidate the sensitivity of difference between the times series of three models and the reference model, the logarithmic difference is calculated at each time step and shown in Figure 8a. The logarithmic difference between the phase-velocity dispersion curves is illustrated in Figure 8b. From Figure 8, it is evident that the difference between each model and the reference model is much higher for their associated time series than for their dispersive properties. In other words, synthetic seismograms reveal more detailed information for the wave propagation differences than just the dispersive properties of the two media.

Nonuniqueness in a Surface-Wave Inverse Problem and the Mitigation Strategy

Model and Assumptions

A synthetic example is presented in which a dispersion curve from a known velocity profile is inverted. The goal of this section is to examine whether we face the nonuniqueness in a typical surface-wave inversion and, if we do, whether the proposed procedure enables us to distinguish the best solution.

A three layer over half-space model is assumed to be representative of the shallow subsurface. Each layer is assumed to have a thickness of 4 m, and the half-space starts from a depth of 12 m. Similar to the previous models, a water level is assumed to be present at the interface between the first layer and the second layer at 4 m depth.

Figure 9 shows the velocity model and the associated phase-velocity dispersion curve used. In real-world data, it is possible to estimate the attenuation in terms of quality factors from the seismic recordings for use in the calculations (Hosseini *et al.*, 2013, 2015; Pezeshk *et al.*, 2013). In this

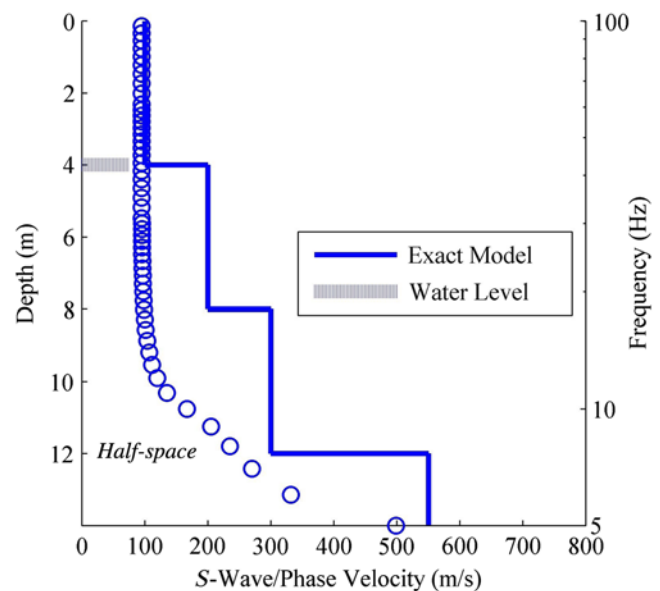


Figure 9. The exact model assumed in the synthetic test as the representative of the shear-wave velocity profile of the subsurface. The color version of this figure is available only in the electronic edition.

study, attenuation effects on the seismograms and dispersion curves are not considered.

Using forward modeling, the phase-velocity dispersion curve is determined and a random 10% noise is added to the dispersion data to generate a realistic synthetic experimental dispersion curve (SEDC) for four modes of propagation. This curve is treated as the experimental dispersion curve that is typically obtained from the field survey; it is used in a linearized damped inversion technique (Aster *et al.*, 2013) and is referred to as an SEDC.

Inversion of the Phase-Velocity Data

Initial velocity profiles for the inversion were constructed by assuming six layers over half-space (each layer

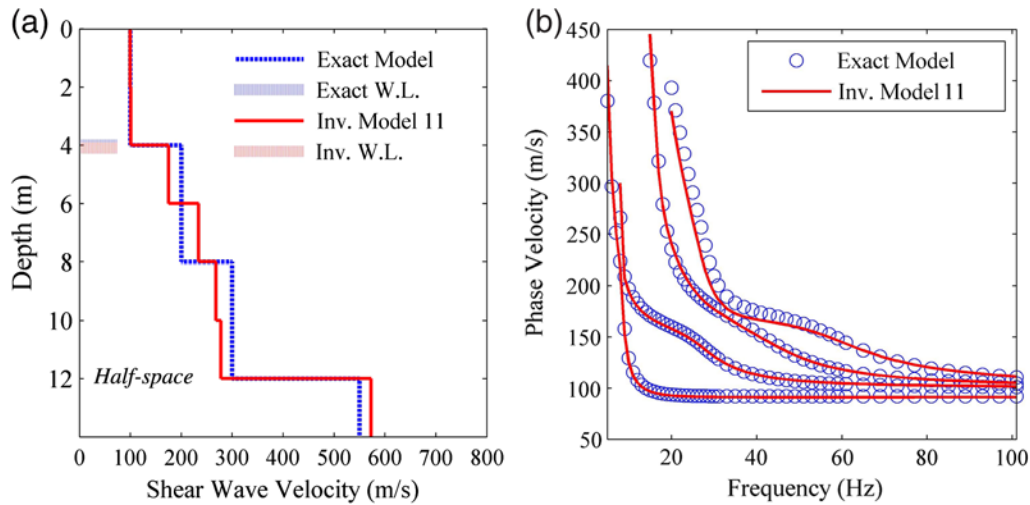


Figure 10. (a) Inverted model 11 (solid line) compared with the exact profile (dashed line). Water levels (W.L.) between the inverted model and the exact one (bold dashed lines) are the same. (b) Dispersion curves for inverted (line) and exact (circle) models are matching well. The color version of this figure is available only in the electronic edition.

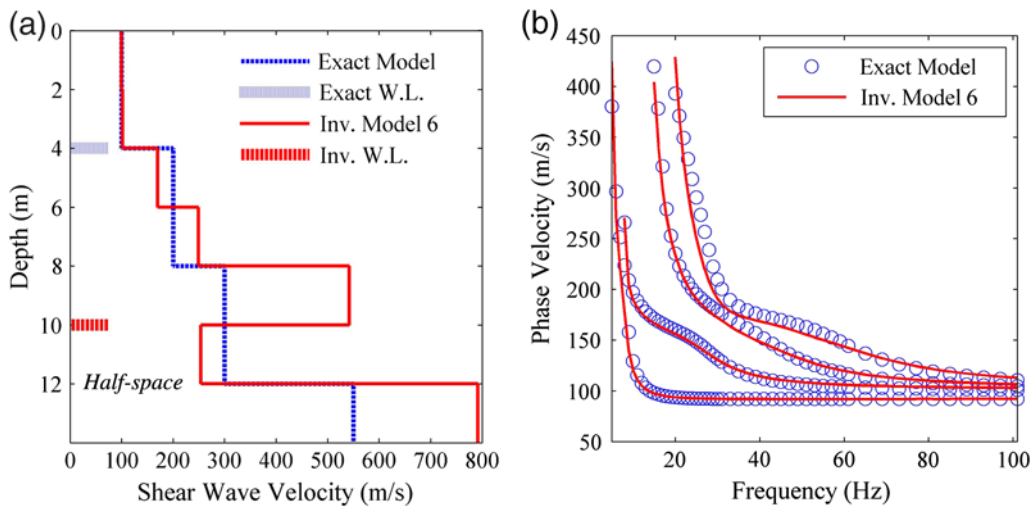


Figure 11. (a) Inverted model 6 (solid line) compared with the exact profile (dashed line). Water levels (W.L.) between the inverted model and the exact one (solid and dashed-bold lines) are different between the profiles. (b) Dispersion curves for inverted (line) and exact (circle) models are matching well up to four modes, despite the difference between the models. The color version of this figure is available only in the electronic edition.

has a thickness of 2 m), and the half-space is 12 m deep. Two initial velocity models are considered in the inversion process, in which the first uses a uniform velocity of 100 m/s for all layers and the second one is a velocity model that linearly increases from 100 m/s at the first layer to 500 m/s at half-space. By combining two initial V_S profiles and eight different levels of the water table, 16 initial velocity profiles were generated and separately inverted.

This section specifically focuses on two successfully inverted models (labeled as profile 6 and 11), for which the dispersion curves are indistinguishable from each other, for up to three higher modes. Figures 10 and 11 present the results of inversion for these two cases. In Figure 10, the

dispersion curve and the velocity structure for profile 11 match well with the SEDC. On the other hand, Figure 11 presents the dispersion and the velocity structure for profile 6, in which the velocity profile is very different from the exact model. The inversion procedure has been successful in terms of matching the theoretical dispersion curve of profiles 6 and 11 with SEDC; however, it fails to preserve the correct velocity profile for inverted profile 6. Therefore, the inversion of the phase-velocity dispersion curve has provided two different inverted velocity profiles, both having a good match between their dispersion and SEDC. Without knowledge of the real V_S model (exact model), it is not possible to choose the final solution between them. Consideration of

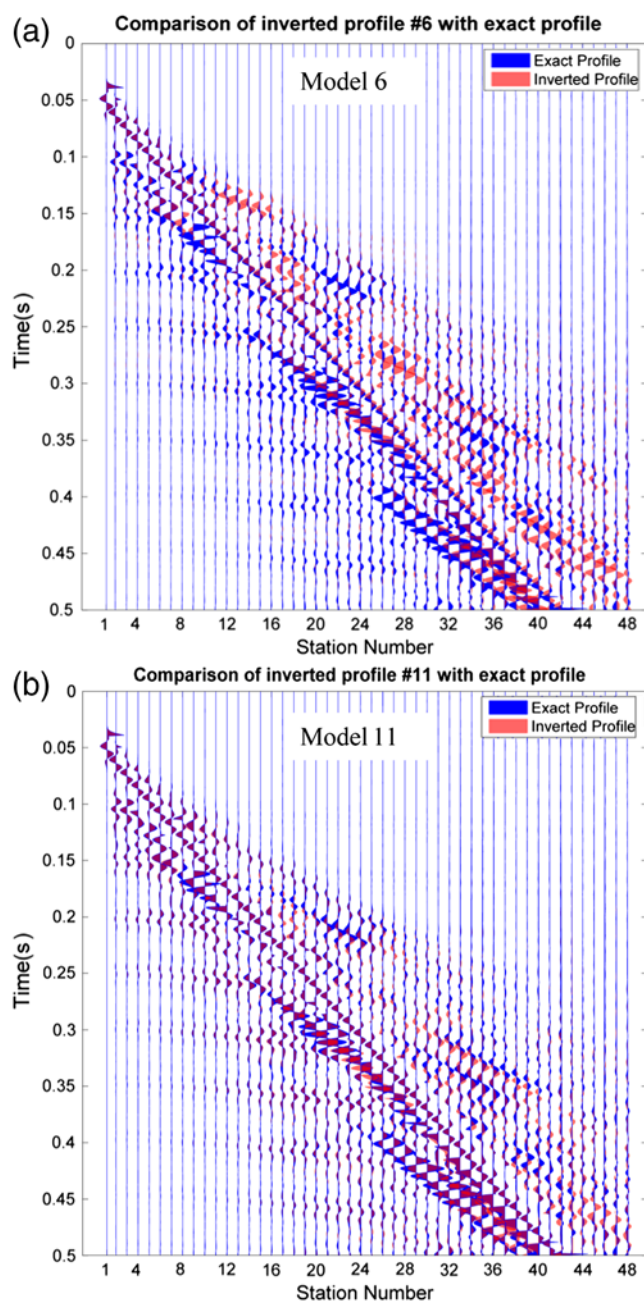


Figure 12. Comparison between synthetic time series from inverted (a) profile 6 and (b) profile 11 with the time series from exact model. The Rayleigh wavetrain is scaled down for clarity. The color version of this figure is available only in the electronic edition.

higher modes does not improve the nonuniqueness, because dispersion curves for both profiles 6 and 11 match the SEDC very closely for up to four modes (Figs. 10b and 11b).

Synthetic and Observed Seismogram Comparison

Synthetic seismograms are generated using velocity models 6 and 11 in 48 imaginary geophones with ~ 1 m spacing. Figure 12 shows synthetic seismograms generated from profiles 6 and 11 plotted on top of the seismograms from the exact profiles. In contrast to the dispersion curves, the time series

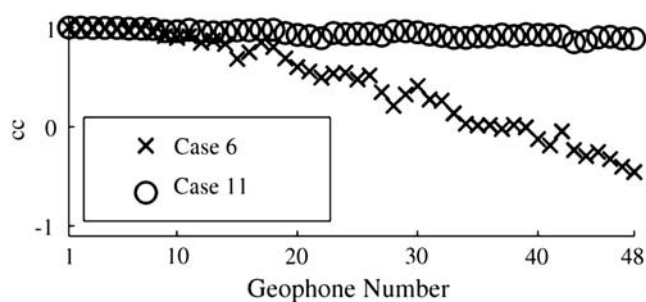


Figure 13. Zero-lag correlation coefficient (cc) for synthetics from models 6 and 11, correlated with the synthetics time series and those from the exact model.

from profiles 6 and 11 are very different and can be used as a tool to distinguish between the two profiles.

For purposes of clarity, Figure 12 has been scaled differently for reflections, refractions, and direct waves compared with the Rayleigh wavetrain. It is evident that profile 11 has a better match between the seismograms and can be selected as the final solution.

To have a quantitative tool for the assessment of similarity between the shapes of the synthetic and observed seismograms, the zero-lag cross-correlation coefficient is used as an indicator of the similarity. Results are provided in Figure 13, which shows that profile number 11 has a better match with observed seismograms at the location of most of the 48 imaginary geophones. Therefore, by comparing the synthetic seismogram it is possible to distinguish between the two different profiles that have similar dispersion curves and overcome the nonuniqueness problem of this synthetic example. Further investigations are necessary to assess the effectiveness of the proposed technique on real-world data. Complexities such as the attenuation structure, attenuation-induced dispersion, and lateral heterogeneity can affect the match quality and the selection of the final profile as shown in Hosseini (2014).

Data and Resources

Synthetic seismograms were computed using the computer program hspec96, and surface-wave dispersion curves were inverted using program surf96, both v.3.3, developed by Robert Herrmann, Department of Earth and Atmospheric Sciences, St. Louis University, St. Louis, Missouri. Program surf96 was modified by the authors to avoid recalculating densities from the compressional-wave velocities as described by Hosseini (2014). The user's guide and other documentation are contained in Computer Programs for Seismology, a software package currently distributed by Herrmann at <http://www.eas.slu.edu/eq/eqccps.html> (last accessed February 2015).

Acknowledgments

We wish to thank anonymous reviewers for their comments, suggestions, and helpful criticisms that greatly improved the manuscript. This research was supported by the U.S. Geological Survey (USGS), Department

of the Interior, under USGS Award Number G13AP00057. The views and conclusions contained in this document are those of the authors and should not be interpreted as necessarily representing official policies, either expressed or implied, of the U.S. Government.

References

- Aster, R. C., B. Borchers, and C. H. Thurber (2013). *Parameter Estimation and Inverse Problems*, Second Ed., Elsevier, Amsterdam, The Netherlands.
- Backus, G., and F. Gilbert (1970). Uniqueness in the inversion of inaccurate gross Earth data, *Phil. Trans. Roy. Soc. Lond.* **266**, 123–192.
- Borcherdt, R. D. (1994). New developments in estimating site effects on ground motion—A new integrated methodology for estimates of site-dependent response spectra, seismic coefficients for site-dependent building code provisions, and predictive GIS maps of strong ground shaking, *Seminar on New Developments in Earthquake Ground Motion Estimation and Implications for Engineering Design Practice ATC 35-1*, Applied Technology Council, Vol. 10, 1–44.
- Bourgoyne, A. T., Jr., K. K. Millheim, M. E. Chenevert, and F. S. Young Jr. (1986). *Applied Drilling Engineering*, SPE Textbook Series 2, Society of Petroleum Engineers, Richardson, Texas.
- Brune, J. N., and J. Dorman (1963). Seismic waves and earth structure in the Canadian shield, *Bull. Seismol. Soc. Am.* **53**, 167–210.
- Cerato, M. (2009). Addressing non-uniqueness in linearized multichannel surface wave inversion, *Geophys. Prospect.* **57**, 27–47.
- Cramer, C., A. Frankel, and C. Muller (2002). A state-of-the-art seismic hazard map with site effects for Memphis, Shelby County, Tennessee, *Proc. 7th U.S. National Conf. on Earthquake Engineering (7NCEE)*, Boston, Massachusetts, 21–25 July 2002.
- Dal Moro, G., and M. Pipan (2007). Joint inversion of surface wave dispersion curves and reflection travel times via multi-objective evolutionary algorithms, *J. Appl. Geophys.* **61**, no. 1, 56–81.
- Dorman, J., and M. Ewing (1962). Numerical inversion of seismic surface wave dispersion data and crust-mantle structure in the New York-Pennsylvania area, *J. Geophys. Res.* **67**, 5227–5241.
- Foti, S., and C. Strobbia (2002). Some notes on model parameters for surface wave data inversion, *Proc. of the Symposium on the Application of Geophysics to Engineering and Environmental Problems (SAGEEP 2002)*, Las Vegas, Nevada, 10–14 February.
- Hosseini, M. (2014). Reducing uncertainties in the velocities determined by inversion of phase velocity dispersion curves using synthetic seismograms, *Ph.D. Dissertation*, The University of Memphis, Memphis, Tennessee.
- Hosseini, M., and F. Aminzadeh (2013). A new model for geomechanical seismicity based reservoir characterization including reservoir discontinuity orientations, *SPE Annual Technical Conference and Exhibition*, New Orleans, Louisiana, 30 September–2 October.
- Hosseini, M., and F. Aminzadeh (2014). A geomechanical approach for microseismic fracture mapping, *Unconventional Resources Technology Conference*, Denver, Colorado, 25–27 August.
- Hosseini, M., and S. Pezeshk (2011a). Comparison of phase velocities and shear-wave velocity inversion results of MASW method obtained by uniform receiver spacing analyzed by SurfSeis package software with non-uniform receiver spacing analyzed by the genetic algorithm inversion scheme, *Annual Meeting of the Geological Society of America*, Minneapolis, Minnesota, 9–12 October.
- Hosseini, M., and S. Pezeshk (2011b). Reliability and efficiency in shear-wave velocity inversion methods and practical considerations for multimodal surface wave inversion technique, *Annual Meeting of the American Geophysical Union*, San Francisco, California, 5–9 December.
- Hosseini, M., and S. Pezeshk (2012a). Improved inversion of surface waves including higher modes of propagation, *Annual Meeting of the Seismological Society of America*, San Diego, California, 17–19 April.
- Hosseini, M., and S. Pezeshk (2012b). Reducing uncertainties in the velocities determined from the inversion of phase velocity dispersion curves using synthetic seismograms, *Annual Meeting of the American Geophysical Union*, San Francisco, California, 3–7 December.
- Hosseini, M., S. Pezeshk, M. Chapman, and A. Conn (2013). Regional investigation of geometrical spreading and quality factor in the central United States, *Annual Meeting of the Seismological Society of America*, Salt Lake City, Utah, 17–19 April.
- Hosseini, M., S. Pezeshk, A. Hajisoltani, and M. Chapman (2015). Investigation of attenuation of the L_g -wave amplitude in the Caribbean region, *Bull. Seismol. Soc. Am.* **105**, no. 2, doi: [10.1785/0120140006](https://doi.org/10.1785/0120140006).
- Hosseini, M., S. Pezeshk, and J. Pujol (2014). Reliable estimation of shear-wave velocity profile by inverting phase velocity dispersion curve and waveform comparison, *Annual Meeting of the Seismological Society of America*, Anchorage, Alaska, 30 April–2 May.
- Kafash, M. H., D. Arellano, S. M. Hosseini, and S. Pezeshk (2013). Feasibility of multi-channel analysis of surface waves (MASW) for evaluating the dynamic properties of geofoam, *Geosynthetics*, Long Beach, California, 10 pp.
- Kanamori, H., and D. L. Anderson (1977). Importance of physical dispersion in surface wave and free oscillation problems: review, *Rev. Geophys. Space Phys.* **15**, 105–112.
- Levshin, A. L., and G. F. Panza (2006). Caveats in multi-modal inversion of seismic surface wavefields, *Pure Appl. Geophys.* **163**, 1215–1233.
- Louie, J. N. (2001). Faster, better: Shear-wave velocity to 100 meters depth from refraction microtremors arrays, *Bull. Seismol. Soc. Am.* **91**, 347–364.
- Mosegaard, K., and M. Sambridge (2002). Monte Carlo analysis of inverse problems, *Inverse Probl.* **18**, R29–R54.
- Nazarian, S. (1984). In situ determination of elastic moduli of soil deposits and pavement systems by spectral-analysis-of-surface-waves method, *Ph.D. Thesis*, University of Texas at Austin, Texas.
- Nazarian, S., and R. Desai (1993). Automated surface wave method: Field testing, *J. Geotech. Eng. ASCE* **119**, no. 7, 1094–1111.
- Nazarian, S., and K. H. Stokoe (1986). In situ determination of elastic moduli of pavement systems by spectral analysis of surface waves method (theoretical aspects), *Research Report 437-2*, Center for Transportation Research, the University of Texas at Austin, Texas.
- Pan, G. S., C. Y. Young, and J. P. Castagna (1994). An integrated target-oriented prestack elastic waveform inversion: Sensitivity, calibration, and application, *Geophysics* **59**, no. 9, 1392–1404.
- Park, C. B., R. D. Miller, and J. Xia (1999). Multichannel analysis of surface waves, *Geophysics* **64**, no. 3, 800–808.
- Pezeshk, S., and M. Zarrabi (2005). A new inversion procedure for spectral analysis of surface waves using a genetic algorithm, *Bull. Seismol. Soc. Am.* **95**, 1801–1808.
- Pezeshk, S., M. Hosseini, M. Chapman, and A. Conn (2013). Study of L_g -wave quality factor in the central United States from horizontal and vertical recorded earthquake seismograms, *Annual Meeting of the American Geophysical Union*, San Francisco, California, 9–13 December.
- Prosser, R. T. (1968). Formal solutions of inverse scattering problems, *J. Math. Phys.* **10**, 1819–1822.
- Renalier, F., D. Jongmans, A. Savvaidis, M. Wathelet, B. Endrun, and C. Cornou (2010). Influence of parameterization on inversion of surface wave dispersion curves and definition of an inversion strategy for sites with a strong V_s contrast, *Geophysics* **75**, no. 6, B197–B209.
- Salama, A., N. Banik, M. Cowman, K. Roberts, A. Glushchenko, M. Egan, A. Gonzalez, E. V. Lunen, and J. Leslie-Panek (2013). Application of surface wave modeling and inversion in Cordova embayment of northeastern British Columbia, *GeoConvention 2013*, Calgary, Canada, 6–10 May 2013.
- Sambridge, M. (1999). Geophysical inversion with a neighbourhood algorithm—I. searching a parameter space, *Geophys. J. Int.* **138**, 479–494.
- Sambridge, M., K. Gallagher, A. Jackson, and P. Rickwood (2006). Trans-dimensional inverse problems, model comparison and the evidence, *Geophys. J. Int.* **167**, 528–542.
- Snieder, R. (1990a). A perturbative analysis of nonlinear inversion, *Geophys. J. Int.* **101**, 545–556.

- Snieder, R. (1990b). The role of the Born approximation in nonlinear inversion, *Inverse Probl.* **6**, 247–266.
- Snieder, R., and J. Trampert (1999). Inverse problems in geophysics, in *Wavefield Inversion*, A. Wirgin (Editor), Springer Verlag, New York, 119–190.
- Snieder, R., and J. Trampert (2000). Linear and nonlinear inverse problems, in *Geomatic Methods for the Analysis of Data in the Earth Sciences*, A. Dermanis, A. Grun, and F. Sanso (Editors), Springer, Berlin, Germany, 93–164.
- Stovall, S. (2010). An improved method for the identification and inversion of multi-mode Rayleigh surface wave dispersion collected from non-uniform arrays utilizing a moving source approach, *Ph.D. Dissertation*, The University of Memphis, Tennessee.
- Strobbia, C., P. Vermeer, A. Laake, A. Glushchenko, and S. Re (2010). Surface waves: Processing, inversion and removal, *First Break* **28**, 85–91.
- Strobbia, C. L., A. Zarkhidze, and R. May (2012). Model-based attenuation for scattered dispersive waves, *74th European Association of Geoscientists and Engineers Conference & Exhibition*, Copenhagen, Denmark, 4–7 June.
- Strobbia, C., A. Zarkhidze, R. May, J. Quigley, and P. Bilsby (2011). Attenuation of aliased coherent noise: Model-based attenuation for complex dispersive waves, *First Break* **29**, 93–100.
- Tran, K. T., and D. R. Hiltunen (2012). One-dimensional inversion of full waveform using genetic algorithm, *J. Environ. Eng. Geophys.* **17**, 197–213.
- Wang, C. Y., and R. B. Herrmann (1980). A numerical study of *P*-, *SV*-, and *SH*-wave generation in a plane layered medium, *Bull. Seismol. Soc. Am.* **70**, 1015–1036.
- Wiggins, R. (1972). The general linear inverse problem: Implication of surface waves and free oscillations for earth structure, *Rev. Geophys. Space Phys.* **10**, no. 1, 251–285.

Department of Civil Engineering
The University of Memphis
Memphis, Tennessee 38152

Manuscript received 10 September 2015;
Published Online 03 November 2015